

Newly identified disorder of copper metabolism caused by variants in *CTR1*, a high-affinity copper transporter

Spyros Batzios^{1,†}, Galit Tal^{2,†}, Andrew T. DiStasio³, Yanyan Peng³, Christiana Charalambous⁴, Paola Nicolaidis⁴, Erik-Jan Kamsteeg⁵, Stanley H. Korman^{2,6}, Hanna Mandel⁷, Peter J. Steinbach⁸, Ling Yi⁹, Summer R. Fair¹⁰, Mark E. Hester^{10,11,12}, Anthi Drousiotou¹³ and Stephen G. Kaler^{3,9,11,*}

¹Department of Paediatric Metabolic Medicine, Great Ormond Street Hospital NHS Foundation Trust, London WC1N 3JH, UK

²Department of Pediatrics B, Metabolic Clinic, Ruth Rappaport Children's Hospital, Rambam Health Care Campus and The Ruth and Bruce Rappaport Faculty of Medicine, Technion–Israel Institute of Technology, Haifa 31096, Israel

³Center for Gene Therapy, Nationwide Children's Hospital, Abigail Wexner Research Institute, and Department of Pediatrics, The Ohio State University College of Medicine, Columbus, OH 43205, USA

⁴Department of Basic and Clinical Sciences, University of Nicosia Medical School, Nicosia 1683, Cyprus

⁵Department of Human Genetics, Radboud University Medical Centre, Nijmegen 6525 GA, The Netherlands

⁶Medical Genetics Institute, Wilf Children's Hospital, Shaare Zedek Medical Center, Jerusalem 9103102, Israel

⁷Department of Genetics, Western Galilee Medical Center, Nahariya 2210001, Israel

⁸Bioinformatics and Computational Biosciences Branch, Office of Cyber Infrastructure and Computational Biology, National Institute of Allergy and Infectious Diseases, National Institutes of Health, Bethesda, MD 20892, USA

⁹Section on Translational Neuroscience, Division of Intramural Research, Eunice Kennedy Shriver National Institute of Child Health and Human Development, National Institutes of Health, Bethesda, MD 20892, USA

¹⁰Steve and Cindy Rasmussen Institute for Genomic Medicine, Nationwide Children's Hospital, Columbus, OH 43205, USA

¹¹Department of Pediatrics, The Ohio State University College of Medicine, Columbus, OH 43210, USA

¹²Department of Neuroscience, The Ohio State University Wexner Medical Center, Columbus, OH 43210, USA

¹³Department of Biochemical Genetics, Cyprus Institute of Neurology and Genetics and Cyprus School of Molecular Medicine, Nicosia 1683, Cyprus

*To whom correspondence should be addressed at: Center for Gene Therapy, Abigail Wexner Research Institute; Room WA3021, Nationwide Children's Hospital, 700 Children's Drive, Columbus, OH 43205-2664. Tel: +1 6147225964; Fax: +1 6147223273; Email: Stephen.Kaler@nationwidechildrens.org

†The authors wish it to be known that, in their opinion, the first two authors should be regarded as joint first authors.

Abstract

The high-affinity copper transporter *CTR1* is encoded by *CTR1* (*SLC31A1*), a gene locus for which no detailed genotype–phenotype correlations have previously been reported. We describe identical twin male infants homozygous for a novel missense variant NM_001859.4:c.284 G > A (p.Arg95His) in *CTR1* with a distinctive autosomal recessive syndrome of infantile seizures and neurodegeneration, consistent with profound central nervous system copper deficiency. We used clinical, biochemical and molecular methods to delineate the first recognized examples of human *CTR1* deficiency. These included clinical phenotyping, brain imaging, assays for copper, cytochrome c oxidase (CCO), and mitochondrial respiration, western blotting, cell transfection experiments, confocal and electron microscopy, protein structure modeling and fetal brain and cerebral organoid *CTR1* transcriptome analyses. Comparison with two other critical mediators of cellular copper homeostasis, *ATP7A* and *ATP7B*, genes associated with Menkes disease and Wilson disease, respectively, revealed that expression of *CTR1* was highest. Transcriptome analyses identified excitatory neurons and radial glia as brain cell types particularly enriched for copper transporter transcripts. We also assessed the effects of Copper Histidinate in the patients' cultured cells and in the patients, under a formal clinical protocol. Treatment normalized CCO activity and enhanced mitochondrial respiration *in vitro*, and was associated with modest clinical improvements. In combination with present and prior studies, these infants' clinical, biochemical and molecular phenotypes establish the impact of this novel variant on copper metabolism and cellular homeostasis and illuminate a crucial role for *CTR1* in human brain development. *CTR1* deficiency represents a newly defined inherited disorder of brain copper metabolism.

Introduction

Copper is a micronutrient essential for numerous cellular functions including processes mediated by a network of copper-dependent enzymes that exploit this metal's facility for electron exchange (1,2). Cellular respiration, antioxidant defense, connective tissue formation, neurotransmitter biosynthesis, neuropeptide amidation and iron homeostasis represent diverse physiological and biochemical processes for which copper ions are critical.

CTR1 is a high-affinity copper uptake protein encoded by *CTR1* (*SLC31A1*) essential for mammalian development and copper homeostasis and also relevant to copper-sensitive malignancies (3–5). Although *CTR1* was initially thought to transport platinum-based anti-cancer drugs as well, compelling evidence to refute this role has been presented (6). A mouse homozygous knockout of *Ctr1* results in prenatal lethality (7,8). Genetic data from normal human populations include six

potential loss-of-function *CTR1* alleles among over 251366 screened (9). Consistent with this low allelic frequency (0.0000238), no descriptions of *CTR1* deficiency exist, although two variant alleles of unknown significance (p.Arg90Gly and p.Val181Leu) were reported in genetic surveys of subjects with possible lysosomal storage disorders or intellectual disability (10–12). Here, we report the primary description of two individuals with *CTR1* deficiency due to a homozygous missense variant and delineate the associated clinical, biochemical and molecular phenotypes.

Results

CTR1 deficiency leads to profound neurodegeneration beginning in early infancy

The patients are monozygotic twins born in Cyprus at 37 weeks gestation to a 31-year-old G2 P1 > 2 female by repeat Caesarean section. Birth weights were 2.78 kg (25th–50th centile relative to gestational age) and 2.35 kg (5th–10th centile relative to gestational age). There was no history of parental consanguinity. The infants were discharged home after 3 days and appeared well for the first 2 months of life.

At 10 weeks of age, both infants became lethargic within 24 h of each other and transient eyelid twitching was noted. At 16 weeks of age, they did not cry or move in response to vaccine injections. At 17 weeks of age, both patients were diagnosed as having complex partial seizures with tonic posturing, eye blinking and head deviations. Electroencephalograms were abnormal and anticonvulsant treatment with phenobarbital, levetiracetam and clonazepam was begun. Temperature instability was noted in both infants. Blood cultures, serum ammonia, plasma and CSF amino acids, plasma acylcarnitines, biotinidase, lysosomal enzymes, homocysteine, vitamin B12 and folate, and urine organic acids and oligosaccharides were normal. Serum lactate was mildly elevated in both twins (1.89 and 2.67 mmol/l; normal range: 0.30–1.30) and CSF lactate more significantly increased (6.22 and 6.67 mmol/l, normal range 1.11–2.78).

At 8 months of age, whole exome sequencing disclosed a homozygous variant, NM_001859.4:c.284 G > A (p.Arg95His), in the *CTR1* gene, which encodes the *CTR1* high-affinity copper transporter [(3,13); Fig. 1A]. *In silico* analyses (CADD and REVEL) predicted a pathogenic effect (14). Both parents were found to be heterozygous for this variant (data not shown). The variant was absent from control populations and was not reported as a benign polymorphism (9). Serum copper was in the normal range for both twins, (92 and 88 $\mu\text{g/dl}$, normal range 80–190 $\mu\text{g/dl}$) as was serum ceruloplasmin (236 and 237 mg/l, normal range 200–640). In contrast, CSF copper was low (0.25 and 0.29 $\mu\text{g/dl}$) compared with previously reported pediatric controls under 3 years of age [0.42–1.04 $\mu\text{g/dl}$, $n = 11$; (15)].

On examination at 9.5 months of age, both infants were still and unresponsive while awake, without

spontaneous movements or vocalization. They showed profound truncal hypotonia with pronounced head lags on pull to sit, appendicular hypertonicity with exaggerated deep tendon reflexes and evidence of cortical blindness (failure to fix and follow visually). They were unable to roll over, sit up independently or grasp objects.

After parental informed consent, the twins enrolled in a Copper Histidinate (CuHis) treatment protocol in accordance with the Israel Ministry of Health urgent compassionate use regulations. CuHis treatment raised the patients' serum copper levels modestly (peak values 95–110 $\mu\text{g/dl}$), and coincided with modest increases in weight, length and head circumference (Fig. 1B). The improved somatic growth is consistent with the physiological response to copper replacement in an intestinal cell-specific *CTR1* knock-out mouse model (16). At 15 months of age, elevated serum alkaline phosphatase was noted in both infants who were found to be profoundly vitamin D-deficient, without radiographic evidence of rickets, and which resolved with oral vitamin D replacement.

By 2 years of age, both twins showed mild clinical improvement in social responsiveness, purposeful smiling and muscle tone. They had strong cries and fixated visually. Oral feeding of liquids and solids had improved considerably. However, both had persistent seizure activity despite multiple anticonvulsant regimens that included corticosteroids for atypical infantile spasms, vigabatrin, oxcarbazepine and topiramate. Twin B was noted to have an increasing head circumference (Fig. 1C) and underwent ventriculoperitoneal shunting for non-obstructive hydrocephalus. The twins remained neurodevelopmentally delayed for age and CuHis treatment in both was stopped after 29 months at the parents' request, with no overt decline in clinical status post-treatment noted. More than 3 years of copper-replacement therapy for patients with this and other inherited copper transport disorders may not be necessary or desirable from a risk:benefit perspective (17).

Structural modeling suggests a molecular basis for impaired Cu transport by CTR1-R95H

A model of the human *CTR1* homotrimer was built with Prime software tools (Schrodinger, LLC) and rendered using MolScript and Raster3D (18,19). The structure of *CTR1* from *Salmo salar* determined by X-ray diffraction provided an excellent template for modeling the human protein; 77% of the modeled residues are identical to the corresponding residues in the template (13). The modeled side chain of Arg95 extends into the conduction pore on the intracellular side of *CTR1* (Fig. 2A), and its charge is balanced by the adjacent Glu91. Consequently, the Arg95His mutation may destabilize the pore geometry at the intracellular end and alter ion conductance. Comparison of salmon and human *CTR1* sequences shows that seven of the eight charged residues (Asp, Glu,

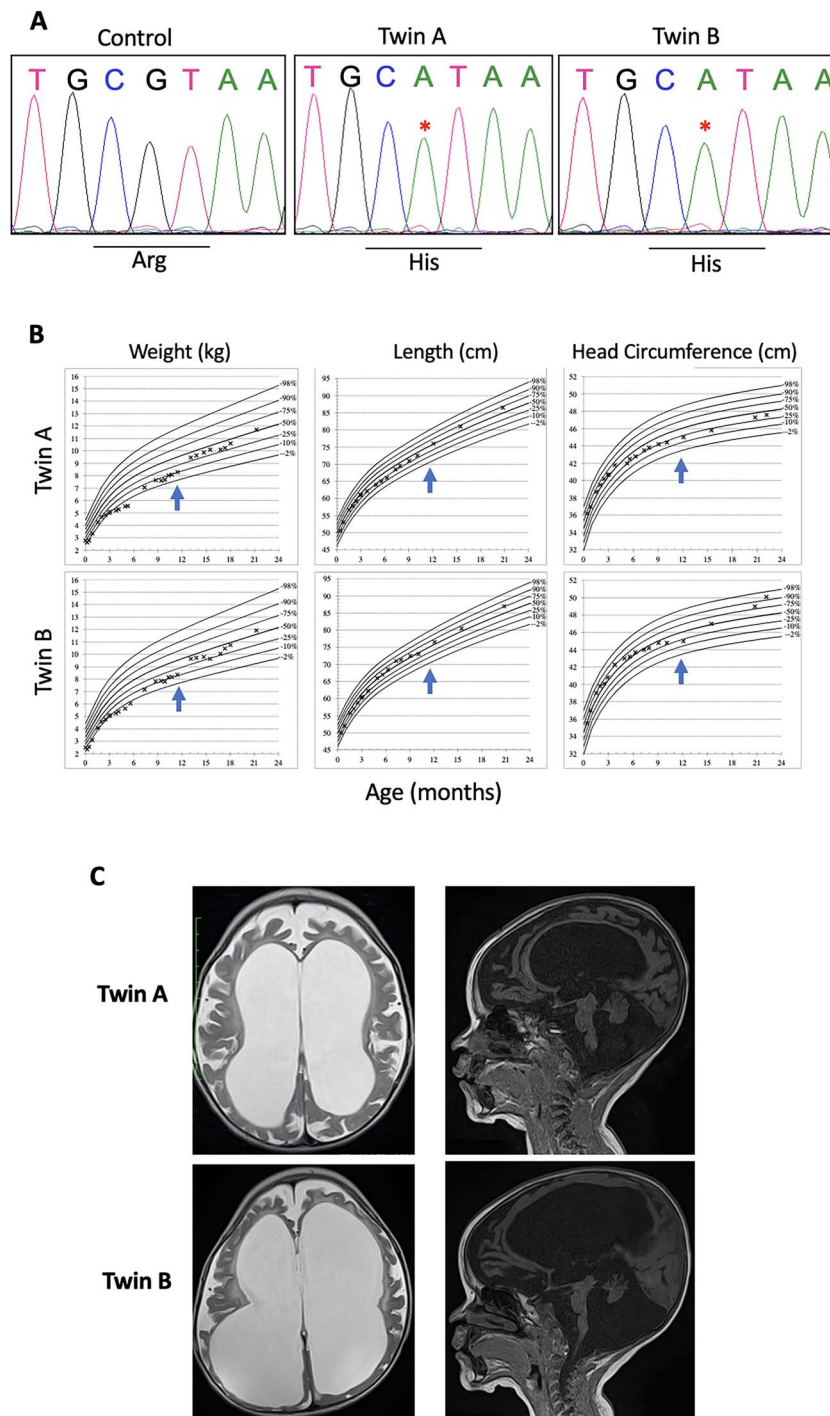


Figure 1. Molecular and clinical findings in twins with $CTR1^{R95H}$. **(A)** DNA sequence analysis of $CTR1$ in the twins. Both parents are heterozygous for the R95H variant (data not shown). **(B)** Growth charts for Twins A and B according to World Health Organization standards for weight, length and head circumference percentiles from birth to 24 months. Blue arrows denote initiation of Copper Histidinate treatment; note increased velocity of weight gain associated with treatment. **(C)** Axial T2-weighted (left) and sagittal T1-weighted (right) brain MRI images at 2 years of age showing ventriculomegaly, and extensive cortical and cerebellar atrophy.

Lys and Arg) on the intracellular side are identical, and the only one that differs (Lys96) corresponds to Arg92 in *S. salar*, preserving the positive charge. The mutation of Arg95 to histidine results in a shorter side chain less likely to carry a positive charge, perturbing the conserved distribution of charge. Moreover, the orientation of the side chain of Arg95 extending into the pore, toward

the other two monomers of the homotrimer (Fig. 2A), amplifies the effect of the mutation. The native affinity of histidine for copper may also affect transport by the mutant homotrimer through creation of an adventitious copper binding site. The orientation of three mutated side chains in the pore, the concomitant change to intracellular charge and the potential for abnormalled

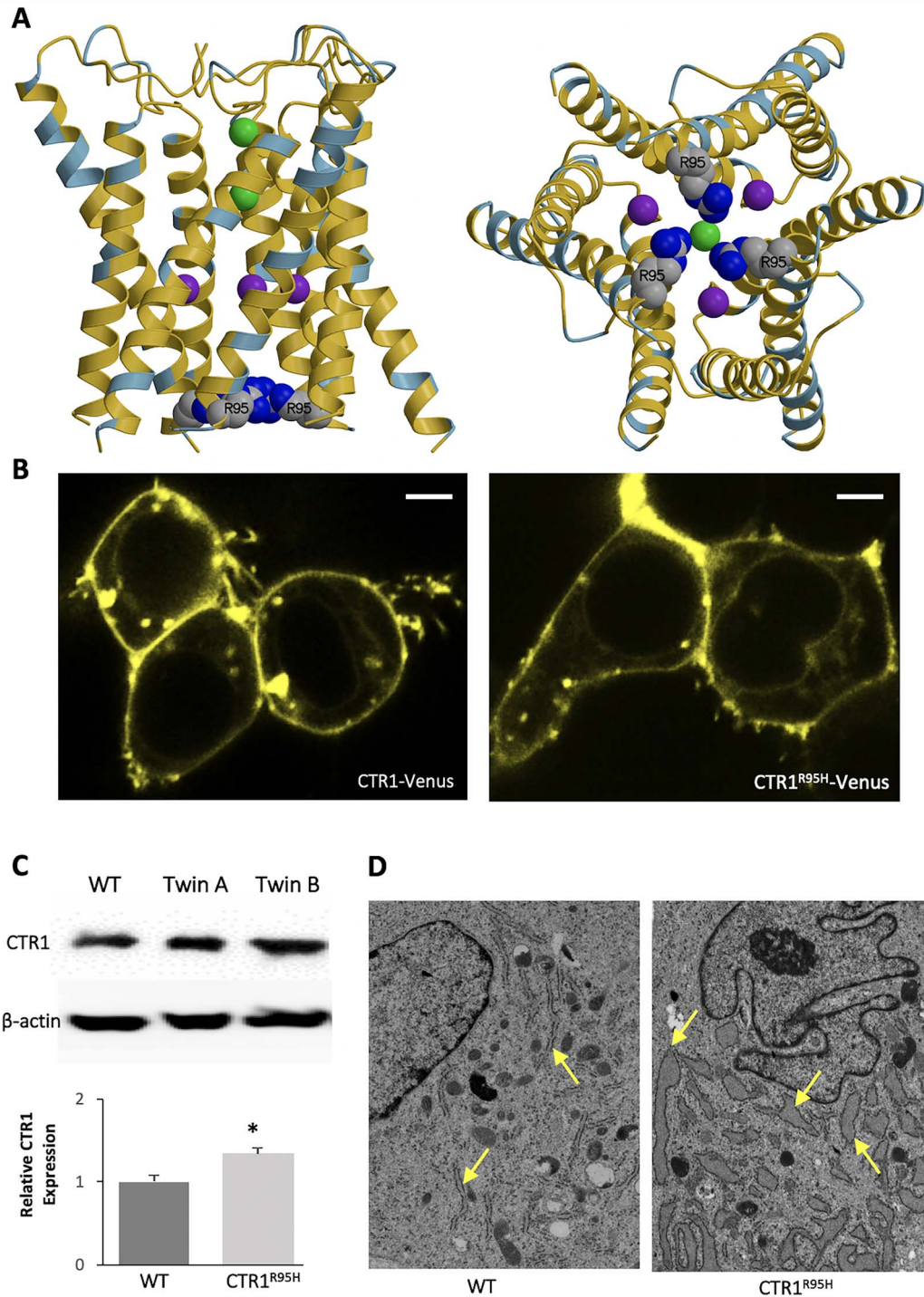


Figure 2. Characterization of CTR1. **(A)** Homology model of the human CTR1 homotrimer. The main chain is colored according to the sequence identity with the template structure (6m98.pdb), gold where identical (77%) and light blue where different. Arg 95 is shown as space-filling. At left is a view in the membrane plane and, on the right, a view from the intracellular side obtained by 90° rotation. Copper and zinc ions are shown as green and purple spheres, respectively. Only crystals grown in conditions containing zinc acetate diffracted X-rays well and allowed the CTR1 structure determination on which this homology model is based (13). CTR1 is not a known transporter of zinc, however. **(B)** Confocal imaging of transfected HEK293T cells, revealing normal plasma membrane localization of CTR1^{R95H}. **(C)** Expression of endogenous CTR1 in primary dermal fibroblasts derived from the affected siblings and from healthy controls. Cell lysates were analyzed by western blotting with the indicated antibodies. A representative blot from among several performed is shown (top), together with a bar graph depicting densitometric analysis of CTR1 expression normalized to beta-actin ($P=0.0185$). Error bars = SEM. **(D)** Representative electron microscopy images of control and patient fibroblasts. Patient fibroblasts exhibit markedly dilated endoplasmic reticulum (yellow arrows).

copper interactions all contribute to the pathogenic impact of Arg95His.

CTR1-R95H mutant allele localizes to the plasma membrane and is associated with dilated ER

We next evaluated the intracellular localization of Venus-tagged CTR1-R95H in transfected HEK293T cells, which revealed predominant positioning at the plasma membrane, and was not significantly different than Venus-tagged wild type CTR1 (Fig. 2B). In western blot analyses of the patients' cultured fibroblasts, expression of the mutant allele appeared slightly increased in comparison with wild type cells (Fig. 2C). Electron microscopy of the patients' fibroblasts revealed strikingly dilated endoplasmic reticulum (Fig. 2D).

Abnormal cellular copper metabolism is ameliorated by CuHis treatment in vitro

Fibroblast copper level was reduced in the patient's cultured cells compared with a normal control cell line (Fig. 3A). Cytochrome c oxidase (CCO) activity, and mitochondrial respiratory chain function were all significantly decreased in the patients' fibroblasts relative to fibroblasts from healthy control individuals (Fig. 3B). Addition of 50 μ M CuHis to the culture media normalized CCO activity (Fig. 3B) and improved overall mitochondrial respiration (Fig. 3C and D).

Fetal brain and human cerebral organoids express Cu transport genes

Next, we assessed representation of CTR1 in human fetal brain cortex and human cerebral organoids (COs) transcriptomes (Fig. 4), utilizing an extensive CO single cell RNA sequencing dataset [(20,21); performed with Seurat v3.2.2 in R v4.0.2; Fig. 4]. This publicly available dataset is comprised of 235 121 single cells from 37 COs across a developmental time window spanning 3–10 weeks. Data were handled using previously described methods (22), and metadata were used to identify cell cluster identities (21). In fetal brain, CTR1 expression was highest in endothelia, excitatory neurons and radial glia (Fig. 4B). Although lacking endothelial cells, COs showed a similar trend of high expression within excitatory neurons and radial glia (Fig. 4D). The latter are specialized cells in the developing nervous system of all vertebrates, and are characterized by long radial processes that guide and facilitate radial migration of newborn neurons from the ventricular zone to the mantle regions of the developing brain (23). Radial glia also function as ubiquitous precursors in the generation of neurons and other glia, and as key elements in patterning and region-specific differentiation of the CNS.

We also analyzed the relative importance of CTR1 in comparison with two well-characterized copper-exporting ATPases, ATP7A and ATP7B (Fig. 5). We first assessed bulk expression levels of ATP7A, ATP7B and CTR1 in CO at two time points, day 93 and day 140 (Fig. 5A), that showed distribution of gene expression

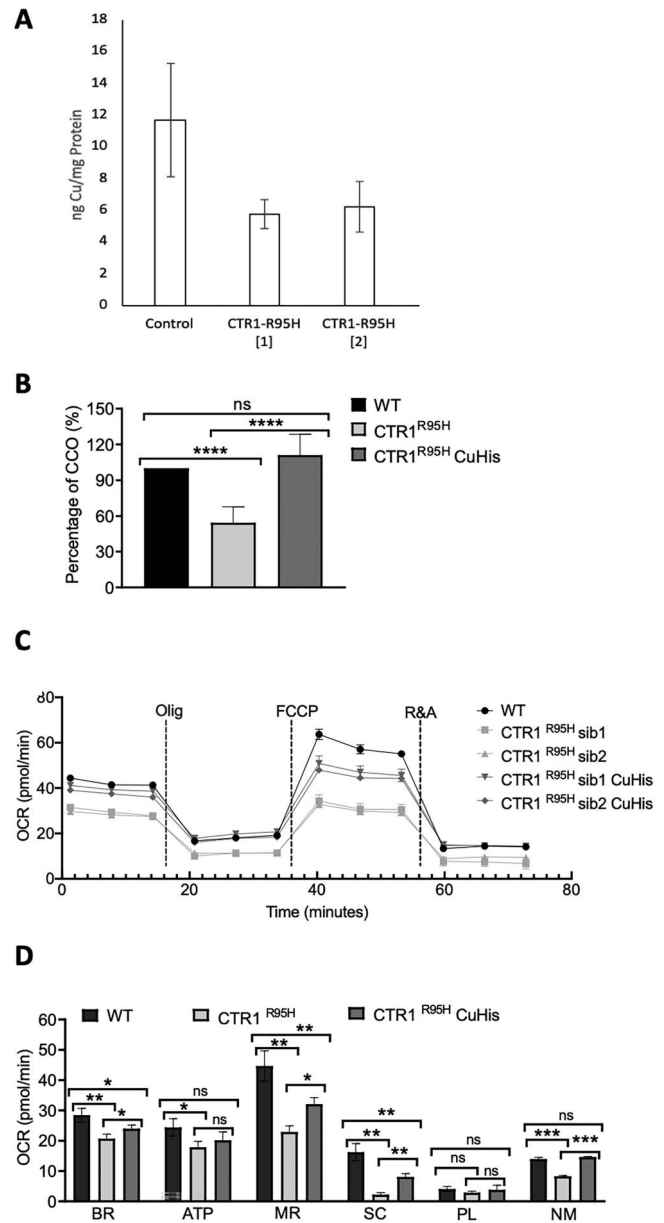


Figure 3. Treatment with copper histidinate (CuHis) enhances mitochondrial function in CTR1^{R95H} fibroblasts. (A) Reduced fibroblast copper content in the patients' cultured fibroblasts compared with normal control cells. Error bars = SD. (B) CCO activity measured spectrophotometrically by loss of ferrocytochrome c following addition of fresh fibroblast lysates normalized to total protein. Results of three independent experiments are shown, with data from two control, both patients' and CuHis-treated both patients' cells pooled. The results indicate reduced activity in the patients' cells ($P < 0.0001$), and increased activity with 50 μ M CuHis treatment. (C,D) Mitochondrial function in primary dermal fibroblasts as measured by a Seahorse XF Analyzer. Results from a representative experiment from among several are depicted as a scatter plot with OCR plotted against time (top). At the time points indicated by dotted lines, the cells were exposed to oligomycin (Olig), carbonyl cyanide 4-(trifluoromethoxy)phenyl-hydrazone (FCCP) and a combination of rotenone and antimycin A (R&A). Mean results from three independent experiments are depicted, with data from affected sibling fibroblasts pooled. The following are plotted: basal respiration (BR, $P = 0.0001$, $P = 0.0299$ after treatment), ATP-linked respiration (ATP, $P = 0.0012$, $P = 0.0419$ after treatment), maximal respiration (MR, $P < 0.0001$, $P < 0.0001$ after treatment), spare capacity (SC, $P < 0.0001$, $P < 0.0001$ after treatment), proton leak (PL, $P = 0.7513$, $P = 0.9884$ after treatment) and non-mitochondrial oxygen consumption (NM, $P = 0.0050$, $P = 0.9122$ after treatment). Error bars = SE

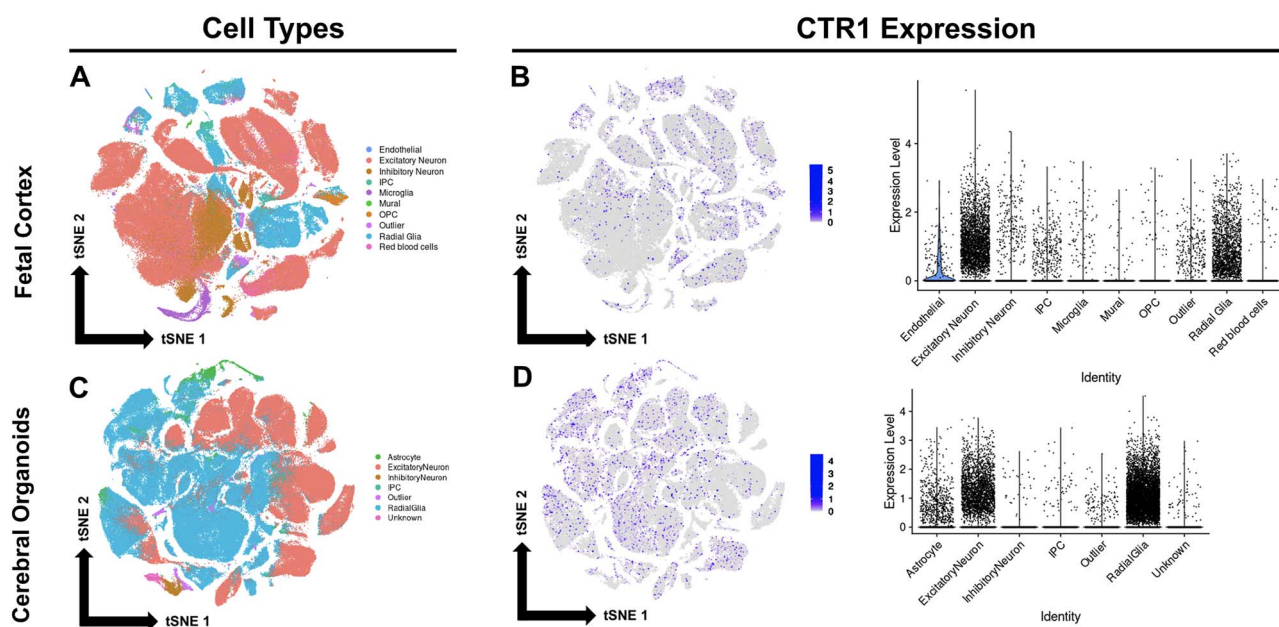


Figure 4. Representation of *CTR1* in fetal brain cortex and CO transcriptomes. (A) t-distributed stochastic neighbor embedding (t-SNE) plot generated from fetal brain cortex single cell RNA sequencing (scRNA-seq) data. Each point on the t-SNE represents a single cell (189 409 cells shown). Cells are color-coded to specify cell type. (B) *CTR1* expression in fetal brain cortex. Left, t-SNE feature plot. Right, violin plots grouped by cell cluster identity. (C) t-SNE plot generated from COs single cell RNA sequencing (scRNA-seq) data. Cells are color-coded to specify cell type. (D) *CTR1* expression in COs. Left, t-SNE feature plot. Right, violin plots grouped by cell cluster identity.

levels for single cells. Each of these data sets represents ~6000 cells (21). These studies indicated highest expression of *CTR1*, followed by *ATP7A* and then *ATP7B* (Fig. 5A). We also surveyed the CO single cell RNA sequencing dataset (19,20) for these three copper transporters (Fig. 5B). These analyses recapitulated the increased expression levels of *CTR1* relative to *ATP7A* and *ATP7B* across all major cell types in these brain organoids.

Discussion

We report identical twin infants homozygous for a pathogenic missense variant (p.Arg95His), in the high-affinity copper transporter *CTR1* who manifest a previously undescribed autosomal recessive syndrome of infantile-onset neurodegeneration. The condition is characterized by hypotonia, global developmental delay, seizures and rapid brain atrophy. These infants' brain imaging findings indicated atrophy greater than in subjects with untreated Menkes disease, an X-linked recessive disorder caused by variants in the copper export protein, *ATP7A* (17,24). Treatment with CuHis improved growth (Fig. 1B) and increased serum Cu levels but was not associated with sustained clinical improvements in the patients. The latter outcome presumably relates, at least in part, to the presence of neurological symptoms and brain injury prior to treatment. CuHis treatment normalized CCO activity and enhanced mitochondrial respiration *in vitro* (Fig. 3), the latter possibly because of enhanced Cu transport kinetics via residual *CTR1* activity, and/or a capacity of CuHis to traverse epithelial plasma membranes by

CTR1-independent mechanisms (Fig. 6A). With improved intracellular copper delivery, activation of copper chaperones and copper-dependent enzymes in *CTR1*-deficient cells is predicted. As for Menkes disease, pre-conditions for optimal clinical efficacy in *CTR1* deficiency include early diagnosis and institution of CuHis treatment before neurological symptom onset (17).

A mouse knock-out model of *CTR1* deficiency resulted in prenatal lethality (7,8). Mice heterozygous for the knocked-out allele showed normal liver and kidney copper levels, presumably reflecting compensatory copper uptake into the blood, and yet profound brain copper deficiency was present. This observation provided insight concerning the subjects of this study, whose blood copper levels were in the normal range but who manifested signs and symptoms of brain copper deficiency. We speculate that gastrointestinal absorption of copper into the blood is not *CTR1*-dependent, whereas brain copper delivery via blood-CSF and/or blood-brain barriers requires *CTR1* (Fig. 6).

We encountered a similar clinical situation in a patient mosaic for an *ATP7A* mutation whose serum copper and neurochemical levels were normal, in contrast to low levels in CSF (15). Based on the pattern of mosaicism noted in mesoderm- and ectoderm-derived tissues, that infant's phenotype strongly indicated that copper entry to the developing brain is primarily choroid plexus-mediated. Previous murine studies indicated intense expression of the mouse *Ctr1* homolog in the choroid plexus beginning at E16.5 and sustained into adulthood (7). We also reported that *ATP7A* is critical for copper delivery from the apical surface of mouse choroid plexus epithelia (24).

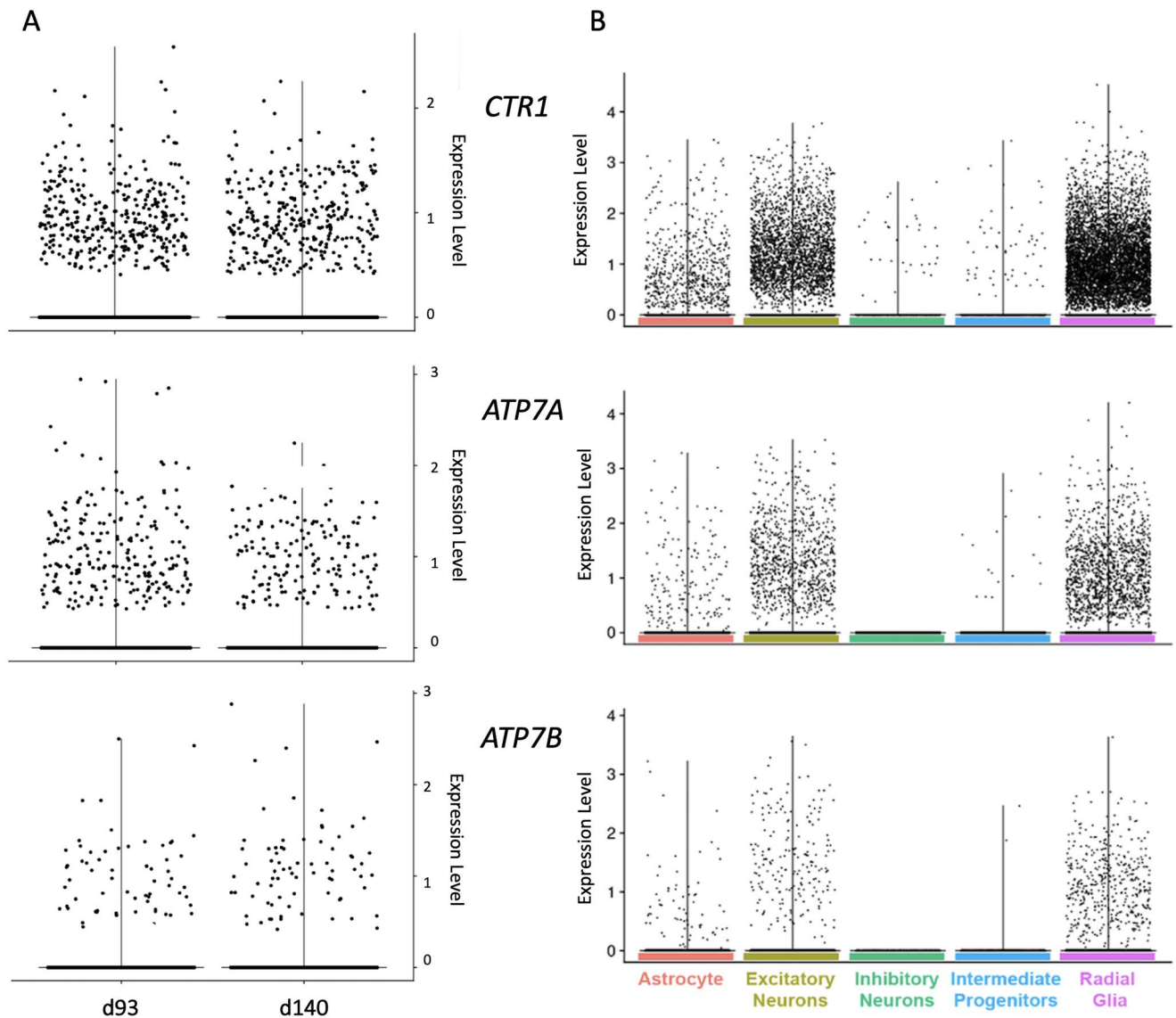


Figure 5. CTR1 expression exceeds copper exporters ATP7A and ATP7B in COs. (A) Bulk expression of CTR1, ATP7A and ATP7B in day 93 and 140 COs. (B) Single cell transcriptomic analysis of CTR1, ATP7A and ATP7B in COs generated from a publicly available dataset of 235 121 single cells from 37 COs cultured across a developmental time window spanning 3–10 weeks (19,20). See text for further details.

These cumulative previous data, in combination with the clinical and biochemical phenotypes of the twins reported here, suggest that CTR1 acts as a copper uptake protein at the basolateral surface of choroid plexus epithelia (Fig. 6B). Convincing evidence for basolateral copper transport by CTR1 in polarized gastrointestinal epithelia also exists (25). This is consistent with normal serum copper levels in these infants with loss of CTR1 whose enterocytic copper acquisition must occur through other mechanisms [(25,26); Fig. 6A].

Analyses of the patients' cultured fibroblasts (Figs 2C, D and 3) confirmed the significant effects of impaired CTR1 function on cellular copper uptake and metabolism. Reductions in intracellular copper, activity of CCO and mitochondrial function potentially explain the patients' lactic acidemia and increased CSF lactate. The distinctively dilated ER (Fig. 2D) suggests the pronounced impact of CTR1 deficiency on oxidative stress,

ER-associated degradation and/or the unfolded protein response (27), which will require further study to dissect.

Recent advances in three-dimensional culture systems have led to the advent of COs that uniquely recapitulate human-specific features of brain development (21). The extensive brain atrophy in these infants (Fig. 1C) and organoid transcriptomic signatures (Figs 4 and 5) imply that CTR1 is less dispensable for normal brain development than even ATP7A (15,24,28). The high single cell expression of CTR1 and other copper transporters in radial glia (Figs 4B, D and 5B) reveal a previously unappreciated aspect of mammalian brain copper metabolism. These intriguing findings will also require further investigation to delineate and elucidate. Direct comparisons of brain protein levels of these copper transporters, which may be more relevant to physiological function, have not been reported. Brain levels of CTR1, ATP7A and ATP7B protein could be

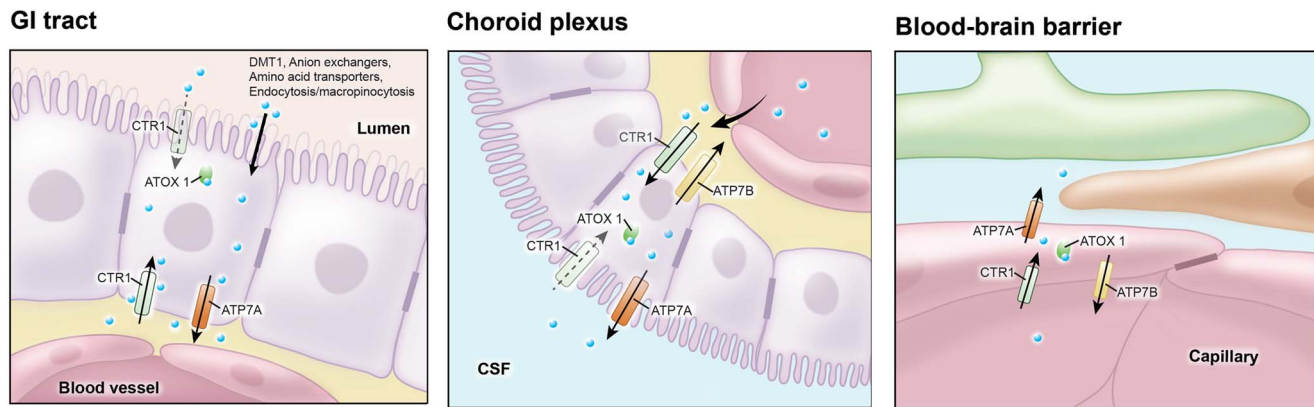


Figure 6. Models of systemic and central nervous system copper uptake. The left panel shows a working model of gastrointestinal copper uptake in which CTR1 is primarily active at the basolateral membranes of enterocytes. CTR1-mediated copper absorption could also occur at the luminal (apical) aspect, however, a number of alternative copper uptake mechanisms have been described. The latter would explain how the infants described here (and mouse models) with defective CTR1 maintain normal blood copper levels. The copper chaperone ATOX1 ferries Cu to the Cu exporter, ATP7A, defective in Menkes disease, which normally mediates copper passage from enterocytes into the blood. The middle panel shows a model of choroid plexus-mediated Cu uptake to the brain in which CTR1 is also localized predominantly at the basolateral aspect of polarized choroid plexus epithelia, reflecting the intense expression documented in this tissue. The well-fenestrated capillaries of the choroid plexuses enable passive Cu exodus from blood to the basolateral epithelial surfaces where CTR1 is presumed to mediate uptake to the epithelial cells. This enables delivery of Cu to ATP7A at the opposite pole, via the cytosolic copper chaperone ATOX1, for delivery to the cerebrospinal fluid (CSF). This model is highly consistent with prior human (15) and murine (24) studies that document copper entry to the developing brain as primarily choroid plexus-mediated. The location and orientation of the Wilson disease gene product, ATP7B, at the basolateral aspect of choroid plexus epithelia are consistent with the toxic brain copper accumulation that occurs in that illness, when untreated (29). The right panel shows a model of copper transport at the blood–brain barrier that we propose is less important based on prior evidence. Tight junctions are present in brain capillary endothelial cells in contrast to choroid plexus and GI tract capillary endothelia, which are well-fenestrated and facilitate passive Cu transport.

influenced by factors other than gene expression, e.g. the rates of copper transport mediated by these proteins.

CTR1 deficiency represents a newly defined inherited disorder of brain copper metabolism. The critical role of CTR1 in the progression of copper-dependent cancers (4,5) further highlights the broad importance of this molecule in human health and disease.

Materials and Methods

Copper treatment

Copper Histidinate was produced at Northwick Park Hospital Pharmacy, London North West Health Care NHS Trust, Watford Road, Harrow HA1 3UJ, UK. Treatment consisted of 125 μg sc twice daily for 3 months and 200 μg sc twice daily for 20 months.

Cell culture

Fibroblast cell lines established from skin biopsy specimens from the two patients and normal control cell lines from ATCC (HDFn) and Coriell Institute (GM03440) were cultured in Dulbecco's modified Eagles medium containing 10% fetal bovine serum, 2-mM glutamine, 100 $\mu\text{g}/\text{ml}$ streptomycin and 100 U/ml penicillin in 5% CO_2 at 37°C. CuHis (50 μM) was added to some cell culture media for ~21 h in certain experiments (e.g., CCO and Seahorse assays).

Copper measurements

CSF copper levels were determined by graphite furnace atomic absorption spectrometry using a transverse heated graphite atomizer. Fibroblast copper quantitation

was measured by inductively coupled plasma mass spectrometry.

Molecular genetic analysis

Whole exome sequencing (Illumina, San Diego Next Seq500 or NovaSeq), read alignment (BWA) and variant calling (GATK) were performed after exome enrichment (Agilent SureSelectQXT Human All Exon). Confirmation of reported variants was performed by Sanger sequencing.

Transfection experiments

Human CTR1 cDNA was obtained by RT-PCR from total RNA extracted from HEK293T cells. Site-directed mutagenesis was used to generate the Arg95His (R95H) mutant allele. After confirming DNA sequence fidelity, CTR1 and CTR1^{R95H} were inserted into pVenus-N1, and HEK293T cells transfected with CTR1/pVenus-N1 or CTR1^{R95H}/pVenus-N1.

Western blotting

Fibroblasts were collected in lysis buffer and proteins electrophoresed through SDS polyacrylamide gels (Invitrogen, Carlsbad), transferred to polyvinylidene fluoride membranes, and incubated with mouse monoclonal antibodies and anti-mouse IgG horseradish peroxidase. Membranes were developed using SuperSignal West Pico Luminol/Enhancer Solution (Pierce, Rockford).

Confocal microscopy

HEK293T cells were transfected as above, examined by confocal microscopy (Zeiss 710, Oberkochen, Germany) 24 h post-transfection and imaged using Zen software.

Electron microscopy

Fibroblasts were post-fixed in EM fixative buffer, washed in 0.1 M Millonig PO4 buffer and post-fixed in 1% osmium tetroxide for 1 h at 4°C. After washing in buffer and dehydration with ethanol, samples were embedded in Araldite 502/Embed 512 (EMS; Hatfield, PA). Ultra-thin (70–90 nm) block sections were counterstained with uranyl acetate 2% (EMS) and lead citrate and imaged with a 30 kV scanning electron microscope (Hitachi, S-4800; Tokyo, Japan).

CTR1 protein modeling

A model of the human CTR1 homotrimer was built with Prime software tools (Schrodinger, LLC) using the crystal structure of CTR1 from *S. salar* (6m98.pdb)¹³ as template. The model was rendered using MolScript and Raster3D (18,19).

Cytochrome C oxidase activity

Cytochrome c oxidase (CCO) activity was measured spectrophotometrically via loss of ferrocytochrome c at 550 nm (CYTOCOX1, Sigma-Aldrich, St. Louis). The reaction rate was calculated by measuring changes in optical density/min at 550 nm using a molar extinction coefficient difference of 21.84 for reduced versus oxidized cytochrome c.

Measurements of mitochondrial respiration

Oxygen consumption rate (OCR) of cultured fibroblasts was measured with a Seahorse XF-96 extracellular flux analyzer (Agilent Technologies, Santa Clara). Basal respiration, ATP production, maximal respiration, proton leak and non-mitochondrial respiration rates in fibroblasts were normalized to cell number. The data were analyzed using XFe Wave software.

CO transcriptome analyses

Single-cell transcriptomic analysis for copper transport genes was performed with Seurat (v3.2.2) in R (v4.0.2) using a publicly available dataset comprised of 235 121 single cells from 37 organoids (20,21). We also analyzed COs generated in our laboratory, as previously described (22).

Statistical analysis

Two-tailed *P*-values were obtained for data from experiments performed in triplicate by using GraphPad software to perform student *t*-tests or chi square analyses.

Acknowledgements

We are grateful to the patients and their parents for participating in this study. We thank Violetta Anastasiadou, Marjo van der Knaap, Yair Anikstair, Anthony Lutton and John Olesik (Trace Element Research Laboratory, School of Earth Sciences, The Ohio State University) and Vincent Schram (NICHD Confocal Microscopy Core) for helpful assistance.

Conflict of Interest statement. The authors report no conflicts of interest.

Funding

Abigail Wexner Research Institute, Nationwide Children's Hospital; Intramural Research Program, Eunice Kennedy Shriver National Institute of Child Health and Human Development, and the Office of Science Management and Operations, National Institute of Allergy and Infectious Diseases, National Institutes of Health.

References

1. Festa, R.A. and Thiele, D.J. (2011) Copper: an essential metal in biology. *Curr. Biol.*, **21**, R877–R883.
2. Inesi, G. (2017) Molecular features of copper binding proteins involved in copper homeostasis. *IUBMB Life*, **69**, 211–217.
3. Zhou, B. and Gitschier, J. (1997) hCTR1: a human gene for copper uptake identified by complementation in yeast. *Proc. Natl. Acad. Sci. U. S. A.*, **94**, 7481–7486.
4. Tsang, T., Posimo, J.M., Gudiel, A.A., Cicchini, M., Feldser, D.M. and Brady, D.C. (2020) Copper is an essential regulator of the autophagic kinases ULK1/2 to drive lung adenocarcinoma. *Nat. Cell Biol.*, **22**, 412–424.
5. Ge, E., Bush, A., Casini, A., Cobine, P., Cross, J., DeNicola, G., Dou, Q.P., Franz, K.J., Gohil, V.M., Gupta, S. et al. (2022) Connecting copper and cancer: from transition metal signaling to metalloplasia. *Nat. Rev. Cancer*, **22**, 102–113.
6. Ivy, K.D. and Kaplan, J.H. (2013) A re-evaluation of the role of hCTR1, the human high-affinity copper transporter, in platinum-drug entry into human cells. *Mol. Pharmacol.*, **83**, 1237–1246.
7. Kuo, Y.M., Zhou, B., Cosco, D. and Gitschier, J. (2001) The copper transporter CTR1 provides an essential function in mammalian embryonic development. *Proc. Natl. Acad. Sci. U. S. A.*, **98**, 6836–6841.
8. Lee, J., Prohaska, J.R. and Thiele, D.J. (2001) Essential role for mammalian copper transporter Ctr1 in copper homeostasis and embryonic development. *Proc. Natl. Acad. Sci. U. S. A.*, **98**, 6842–6847.
9. Karczewski, K.J., Francioli, L.C., Tiao, G., Cummings, B.B., Alföldi, J., Wang, Q., Collins, R.L., Laricchia, K.M., Ganna, A., Birnbaum, D.P. et al. (2020) The mutational constraint spectrum quantified from variation in 141,456 humans. *Nature*, **581**, 434–443.
10. Najmabadi, H., Hu, H., Garshasbi, M., Zemojtel, T., Abedini, S.S., Chen, W., Hosseini, M., Behjati, F., Haas, S., Jamali, P. et al. (2011) Deep sequencing reveals 50 novel genes for recessive cognitive disorders. *Nature*, **478**, 57–63.
11. Jadot, M., Boonen, M., Thirion, J., Wang, N., Xing, J., Zhao, C., Tannous, A., Qian, M., Zheng, H., Everett, J.K. et al. (2017) Accounting for protein subcellular localization: a compartmental map of the rat liver proteome. *Mol. Cell. Proteomics*, **16**, 194–212.
12. Wang, N., Zhang, Y., Gedvilaite, E., Loh, J.W., Lin, T., Liu, X., Kumar, D., Donnelly, R., Raymond, K., Schuchman, E.H. et al. (2017) Using whole-exome sequencing to investigate the genetic bases of lysosomal storage diseases of unknown etiology. *Hum. Mutat.*, **38**, 1491–1499.
13. Ren, F., Logerman, B.L., Zhang, X., Liu, Y., Thiele, D.J. and Yuan, P. (2019) X-ray structures of the high-affinity copper transporter Ctr1. *Nat. Commun.*, **10**, 1386.
14. Ioannidis, N.M., Rothstein, J.H., Pejaver, V., Middha, S., McDonnell, S.K., Baheti, S., Musolf, A., Li, Q., Holzinger, E., Karyadi,

- D. et al. (2016) REVEL: an ensemble method for predicting the pathogenicity of rare missense variants. *Am. J. Hum. Genet.*, **99**, 877–885.
15. Donsante, A., Johnson, P., Jansen, L.A. and Kaler, S.G. (2010) Somatic mosaicism in Menkes disease suggests choroid plexus-mediated copper transport to the developing brain. *Am. J. Med. Genet. A*, **152A**, 2529–2534.
 16. Nose, Y., Kim, B.E. and Thiele, D.J. (2006) Ctr1 drives intestinal copper absorption and is essential for growth, iron metabolism, and neonatal cardiac function. *Cell Metab.*, **4**, 235–244.
 17. Kaler, S.G., Holmes, C.S., Goldstein, D.S., Tang, J., Godwin, S.C., Donsante, A., Liew, C.J., Sato, S. and Patronas, N. (2008) Neonatal diagnosis and treatment of Menkes disease. *N. Engl. J. Med.*, **358**, 605–614.
 18. Kraulis, P.J. (1991) MOLSCRIPT: a program to produce both detailed and schematic plots of protein structures. *J. Appl. Crystallogr.*, **24**, 946–950.
 19. Merritt, E.A. and Bacon, D.J. (1997) Raster3D: photorealistic molecular graphics. *Methods Enzymol.*, **277**, 505–524.
 20. Stuart, T., Butler, A., Hoffman, P., Hafemeister, C., Papalexi, E., Mauck, W.M., 3rd, Hao, Y., Stoeckius, M., Smibert, P. and Satija, R. (2019) Comprehensive integration of single-cell data. *Cell*, **177**, 1888–1902e21.
 21. Bhaduri, A., Andrews, M.G., Mancia Leon, W., Jung, D., Shin, D., Allen, D., Jung, D., Schmunk, G., Haeussler, M., Salma, J. et al. (2020) Cell stress in cortical organoids impairs molecular subtype specification. *Nature*, **578**, 142–148.
 22. Fair, S.R., Julian, D., Hartlaub, A.M., Pusuluri, S.T., Malik, G., Summerfied, T.L., Zhao, G., Hester, A.B., Ackerman, W.E., 4th, Hollingsworth, E.W. et al. (2020) Electrophysiological maturation of cerebral organoids correlates with dynamic morphological and cellular development. *Stem Cell Reports.*, **15**, 855–868.
 23. Campbell, K. and Götz, M. (2002) Radial glia: multi-purpose cells for vertebrate brain development. *Trends Neurosci.*, **25**, 235–238.
 24. Donsante, A., Yi, L., Zerfas, P., Brinster, L.R., Sullivan, P., Goldstein, D.S., Prohaska, J., Centeno, J.A., Rushing, E. and Kaler, S.G. (2011) ATP7A gene addition to the choroid plexus results in long-term rescue of the lethal copper transport defect in a Menkes disease mouse model. *Mol. Ther.*, **19**, 2114–2123.
 25. Zimnicka, A.M., Maryon, E.B. and Kaplan, J.H. (2007) Human copper transporter hCTR1 mediates basolateral uptake of copper into enterocytes: implications for copper homeostasis. *J. Biol. Chem.*, **282**, 26471–26480.
 26. Pierson, H., Yang, H. and Lutsenko, S. (2019) Copper transport and disease: what can we learn from organoids? *Annu. Rev. Nutr.*, **39**, 75–94.
 27. Sun, S., Shi, G., Han, X., Francisco, A.B., Ji, Y., Mendonça, N., Liu, X., Locasale, J.W., Simpson, K.W., Duhamel, G.E. et al. (2014) Sel1L is indispensable for mammalian endoplasmic reticulum-associated degradation, endoplasmic reticulum homeostasis, and survival. *Proc. Natl. Acad. Sci. U. S. A.*, **111**, E582–E591.
 28. Kaler, S.G. (2011) ATP7A-related copper transport diseases-emerging concepts and future trends. *Nat. Rev. Neurol.*, **7**, 15–29.
 29. Bandmann, O., Weiss, K.H. and Kaler, S.G. (2015) Neurological effects of Wilson disease and other copper metabolism disorders. *Lancet Neurol.*, **14**, 103–113.